Electronic Supplementary Material (ESI) for ChemComm.

Supporting Information

Inside-Mode Indium Oxide/Carbon Nanotube for Efficient Carbon Dioxide Electroreduction by Suppressing Hydrogen Evolution

Haichuan He,[ab] Congcheng Yang,[a] Liu Deng,*[ab] Jian Wu,[a] Fei Chen,[a] Jianhan Huang [a] and You-Nian Liu *[ab]

[a] Hunan Provincial Key Laboratory of Micro & Nano Materials Interface Science, College of Chemistry and Chemical Engineering, Central South University, Changsha, Hunan 410083, China

[b] State Key Laboratory for Powder Metallurgy, Central South University, Changsha, Hunan 410083, China

1. Experimental Section

Materials: Indium nitrate hydrate ($In(NO_3)_3 \cdot xH_2O$), 1,4-benzenedicarboxylic acid (H_2BDC), N,N-dimethyl-formamide (DMF), ethanol, and potassium bicarbonate ($KHCO_3$) were purchased from Sinopharm (Shanghai, China). Dimethyl sulfoxide (DMSO), multiwalled carbon nanotubes (MWCNTs), Nafion solution, and Nafion@117 film were obtained from Sigma-Aldrich. CO_2 (99.99%), N2 (99.99%) were purchased from Saizhong Gas (Changsha, China).

Materials synthesis: MWCNTs@MIL-68 precursor was synthesized by a typical method with slight modifications. Briefly, 90 mg of $In(NO_3)_3 \cdot xH_2O$ and 0.9 mg of MWCNTs were dissolved in 40 mL of DMF and stirred for 2 h. Then, 110 mg of H_2BDC were added into the above solution under stirring for 10 min. Subsequently, the solution was kept standing in an oil bath at 120 °C for 30 min. After the completion of the reaction, the precipitate was washed with ethanol for three times and dried at 60 °C for 12 h. MIL-68 hexagonal prism was synthesized with the same method as MWCNTs@MIL-68 but without addition of MWCNTs. MWCNTs@In_2O_3 composite was synthesized by pyrolysis of MWCNTs@MIL-68 hexagonal prisms in a tube furnace at 350 °C under air atmosphere for 1 h. MIL-68-derived-In_2O_3 was prepared by the same procedure using MIL-68. MWCNTs/In_2O_3 is physically mixed MIL-68-derived In_2O_3 and MWCNTs.

Characterizations of materials: Microstructures were determined with a Helios NanoLab 600i Dual Beam FIB/FE-SEM (FEI, USA). The transmission electron microscopy (TEM) images were obtained on a FEI Titan G2 60–300 (FEI, USA) with spherical aberration correction. Powder X-ray diffraction (XRD) patterns were identified by a Rigaku D/max 2550 X-ray diffractometer with Cu Kα radiation (λ=0.15418 nm) (Rigaku, Japan). X-ray photoelectron spectroscopy (XPS) were gained from ESCALAB 250Xi (Thermo Fisher Scientific, USA) with Al Kα radiation as the X-ray source.

Electrochemical measurements: All the electrochemical measurements were evaluated in CO_2-saturated 0.5 M $KHCO_3$ solution within a Nafion-membrane separated airtight H-type cell. The Ag/AgCl electrode and Pt electrode were used as the reference electrode and counter electrode, respectively. The electrocatalysts were modified on carbon papers of 1 cm × 1 cm as working electrode. Typically, 10 mg of electrocatalyst and 50 μL of Nafion solution (5 wt%) were dispersed in 5 mL of ethanol by sonicating for 20 min to form a homogeneous catalyst ink. Then, 500 μL the catalyst ink was uniformly deposited on carbon papers to act as the working electrode. The potential was calculated to the reversible hydrogen electrode (RHE).

$$E(\text{RHE}) = E(\text{Ag/AgCl}) + 0.1989\ \text{V} + 0.059 \times \text{pH}.$$

Before the CO_2 reduction experiments, the solution was bubbled with gas (CO_2 or N_2) for at least 30 min to make the aqueous solution saturated. The linear sweep voltammetry (LSV) was performed in CO_2-saturated and N_2-saturated 0.5 M $KHCO_3$ aqueous solution from 0 to −1.2 V vs. RHE at a scan rate of 50 mV s^{-1}. The electrochemical CO_2 reduction reaction was carried out in CO_2-saturated 0.5 M $KHCO_3$ electrolyte (pH = 7.2) in the potential range of −0.6 to −1.2 V vs. RHE at room temperature. Cyclic voltammogram measurements were conducted from 0.2 to 0.3 V vs. RHE with various scan rates (5, 10, 15, 20, 25 and 30 mV s^{-1}) to obtain the double layer capacitance (C_{dl}). The electrochemically active surface area (ECSA) of the working electrodes were calculated according to the following equation:

$$\text{ECSA} = R_f S,$$

where R_f is the roughness factor, S is the geometric area of the working electrode. The R_f can be determined by the relation $R_f = C_{dl}/60\ \mu\text{F cm}^{-1}$ based on the C_{dl} of a smooth oxide surface.

Computational Method: Gibbs free energies of electrochemical CO_2 reduction reaction states were performed using codes from Vienna Ab-initio Simulation Package (VASP),[1, 2] taking advantage of the density functional theory (DFT) with the Projected Augmented Wave (PAW) method.[3] The revised Perdew-Burke-Ernzerhof (RPBE) functional was used to describe the exchange and correlation effects.[4-6] For all the geometry optimizations, the cutoff energy was set to be 500 eV. The Monkhorst-Pack method were set to be 2 × 2× 1 for performing the calculations on In_2O_3 and MWCNTs@ In_2O_3. A 15 Å vacuum thickness was added in the z-direction of the simulation box, preventing the interactions between the adjacent slabs.

In aqueous conditions, the reduction of CO_2 to produce $HCOO^-$ could occur in the following three elementary steps:

$CO_2 + e^- + * \rightarrow CO_2*^-$

$CO_2*^- + (H^+ + e^-) \rightarrow HCOO*^-$

$HCOO*^- \rightarrow HCOO^- + *$

where * denotes the active sites on the catalyst surface. The computational hydrogen electrode (CHE) model proposed by Norskov et al. was used to calculate the free energies of the reaction intermediates, based on which the free energy of an adsorbed species is defined as, [7]

$$\Delta G_{ads} = \Delta E_{ads} + \Delta E_{ZPE} - T\Delta S_{ads} + \int C_P dT$$

where ΔE_{ads} is the electronic adsorption energy, ΔE_{ZPE} is the zero-point energy difference between adsorbed and gaseous species, $T\Delta S_{ads}$ is the corresponding entropy difference between these two states, and $\int C_P dT$ is the enthalpy correction. The electronic binding energy is referenced as graphene for each C atom, ½ H_2 for each H atom, and (H_2O-H_2) for each O atom, plus the energy of the clean slab. The corrections of zero-point energy, entropy, and enthalpy of adsorbed and gaseous species can be found in the supporting information.

2. Supplementary Figures

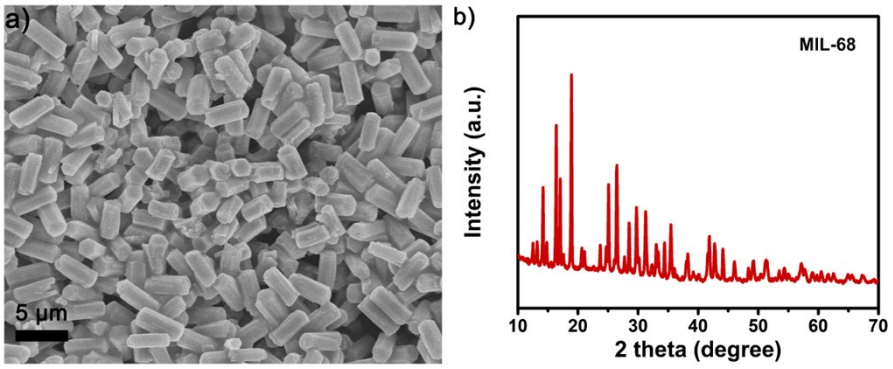

Fig. S1 a) SEM image and b) XRD pattern of the MIL-68 hexagonal prisms.

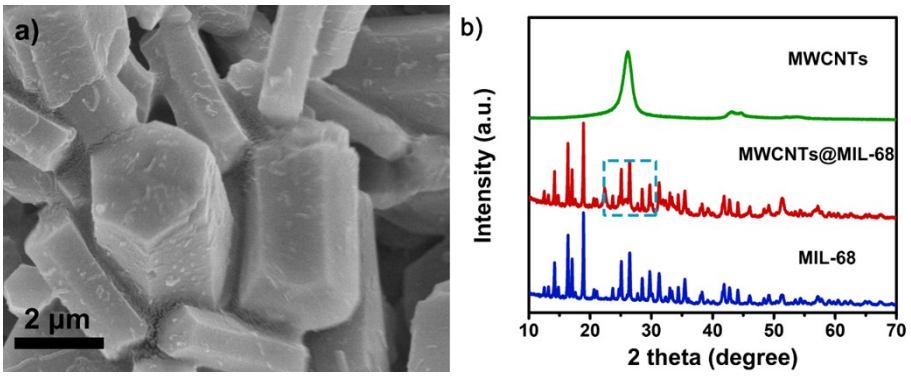

Fig. S2 a) SEM image and b) XRD pattern of MWCNTs@MIL-68.

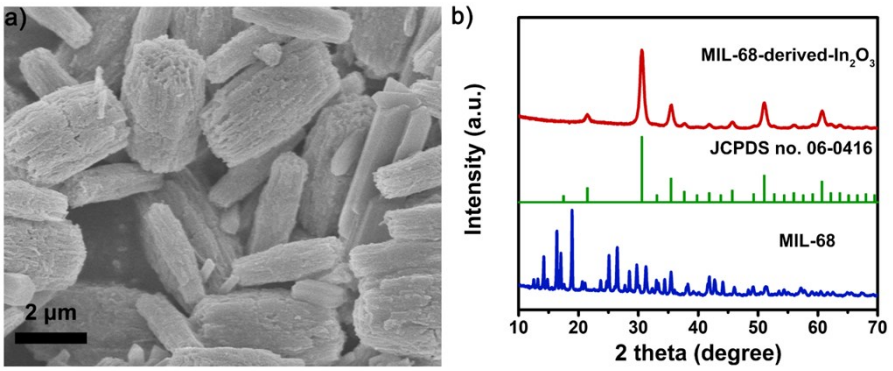

Fig. S3 a) SEM image and b) XRD pattern of MIL-68-derived-In_2O_3.

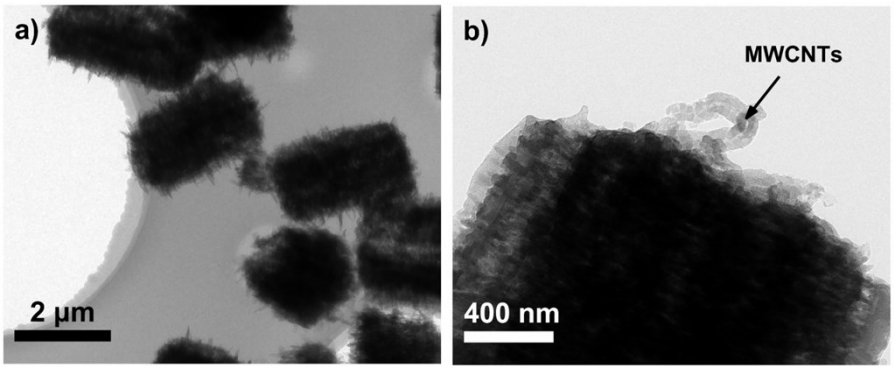

Fig. S4 TEM image of MWCNTs@In_2O_3.

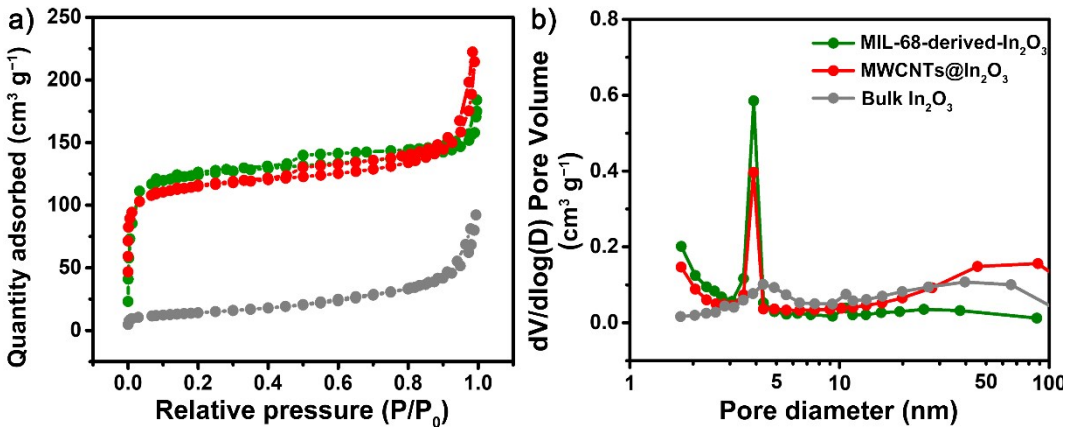

Fig. S5 a) N_2 adsorption-desorption isotherms and b) Pore size distributions of MIL-68-derived-In_2O_3, MWCNTs@In_2O_3 and bulk In_2O_3.

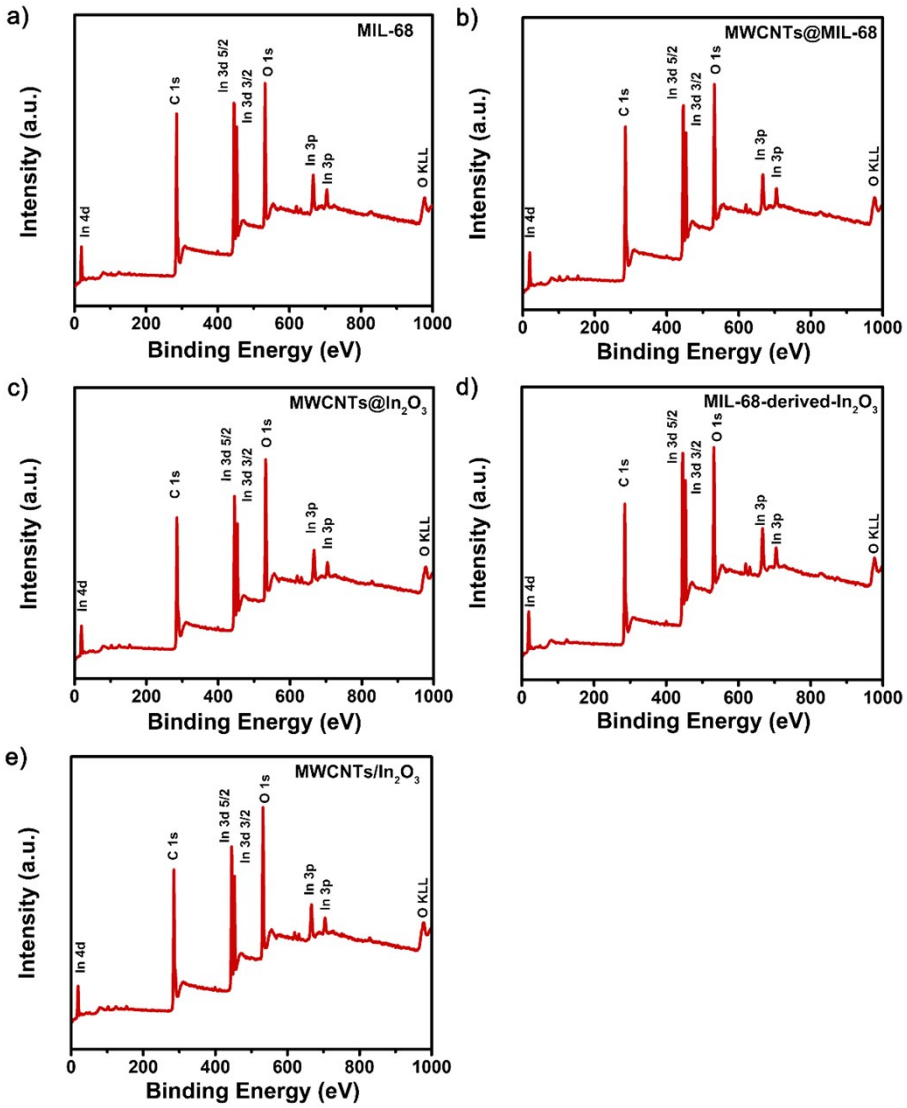

Fig. S6 XPS spectrum of a) MIL-68, b) MWCNTs@MIL-68, c) MWCNTs@In_2O_3, d) MIL-68-derived-In_2O_3 and e) MWCNTs/In_2O_3.

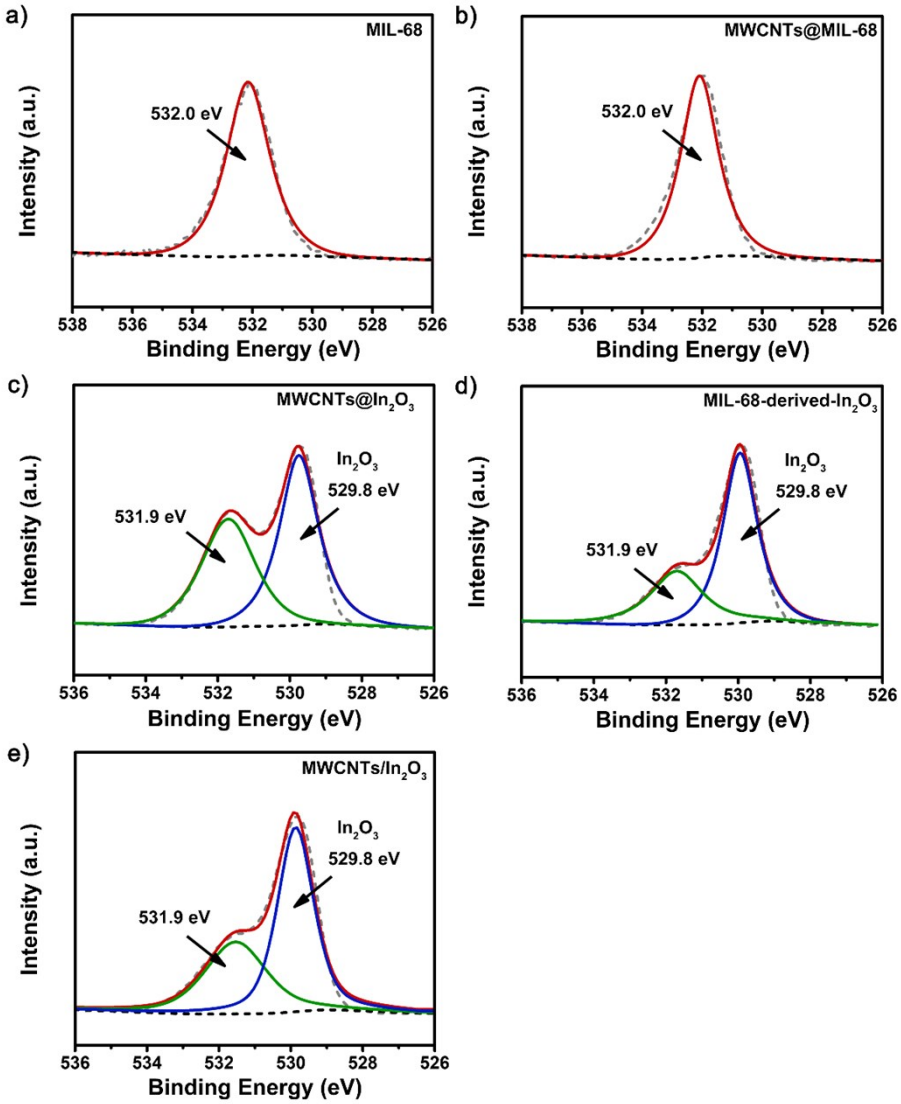

Fig. S7 O 1s XPS spectrum of a) MIL-68, b) MWCNTs@MIL-68, c) MWCNTs@In_2O_3, d) MIL-68-derived-In_2O_3 and e) MWCNTs/In_2O_3.

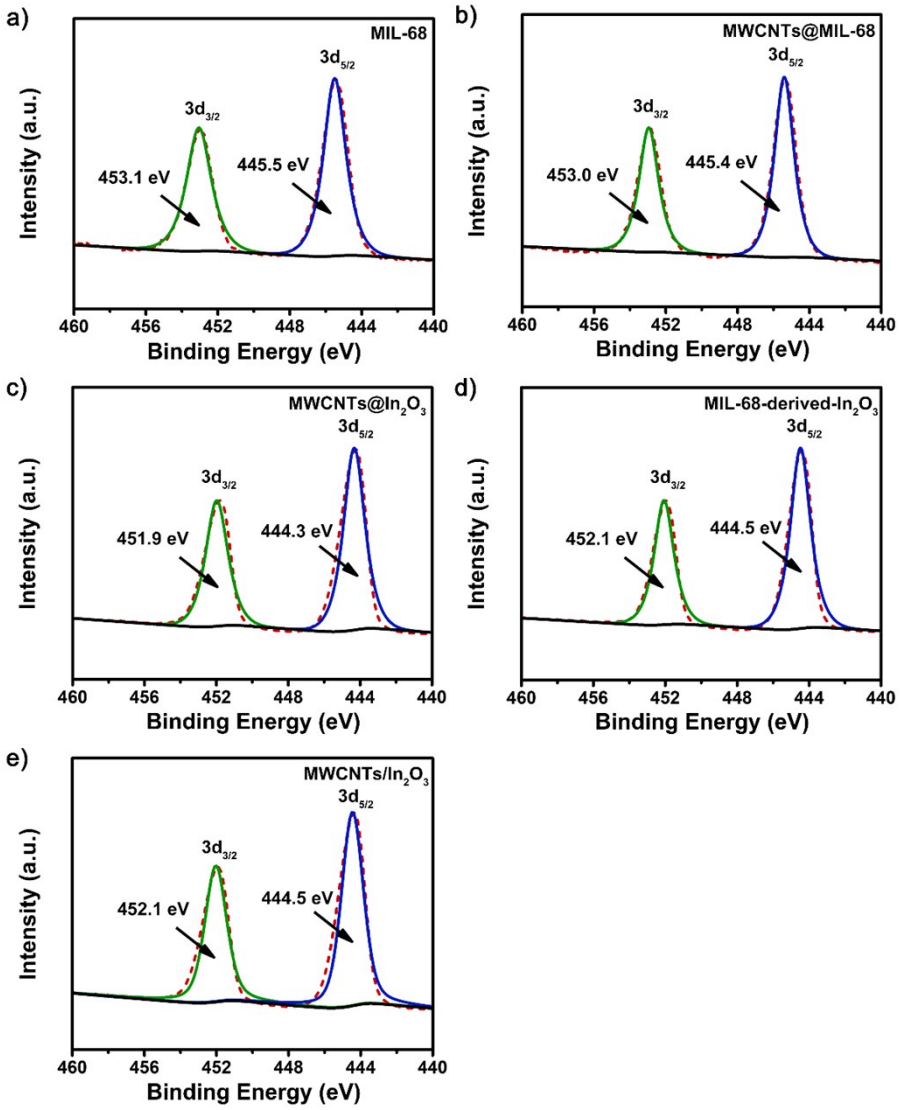

Fig. S8 In 3d XPS spectrum of a) MIL-68, b) MWCNTs@MIL-68, c) MWCNTs@In_2O_3, d) MIL-68-derived-In_2O_3 and e) MWCNTs/In_2O_3.

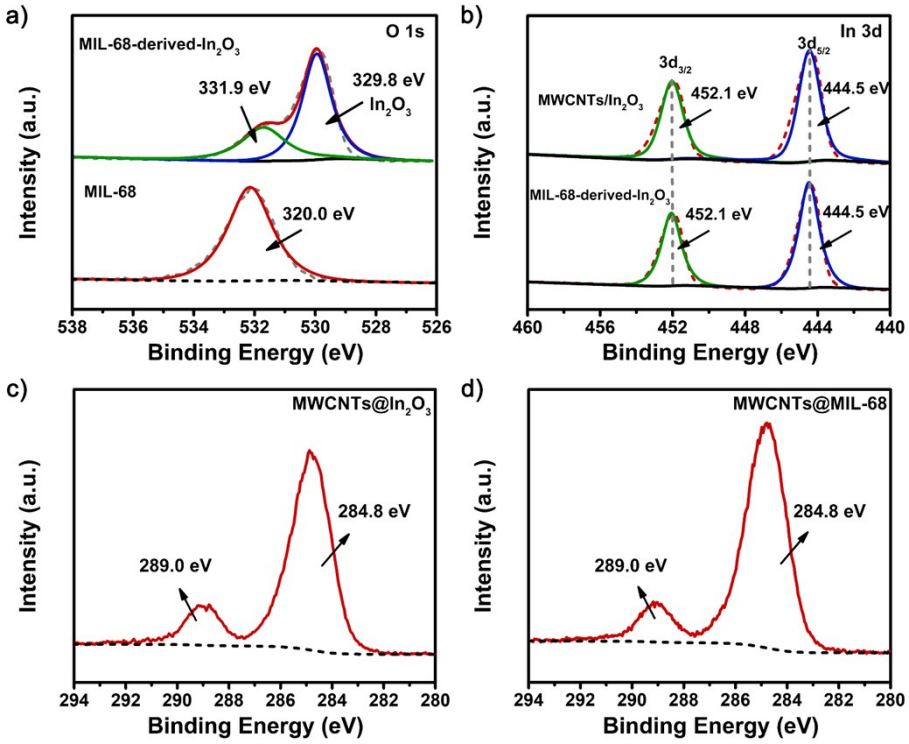

Fig. S9 a) O 1s XPS spectra of MIL-68 and MIL-68-derived-In_2O_3. b) In 3d XPS spectra of MWCNTs/In_2O_3 and MIL-68-derived-In_2O_3. C 1s XPS spectra of c) MWCNTs@In_2O_3 and d) MWCNTs@MIL-68.

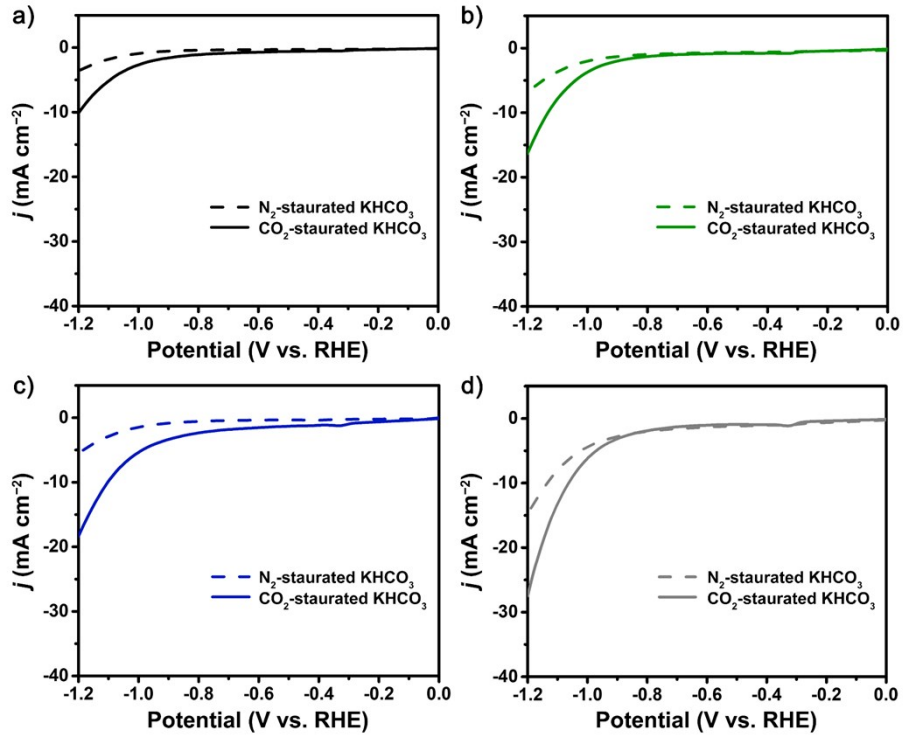

Fig. S10 LSV curves of a) MIL-68, b) MWCNTs@MIL-68, c) MIL-68-derived-In_2O_3 and d) MWCNTs/In_2O_3.

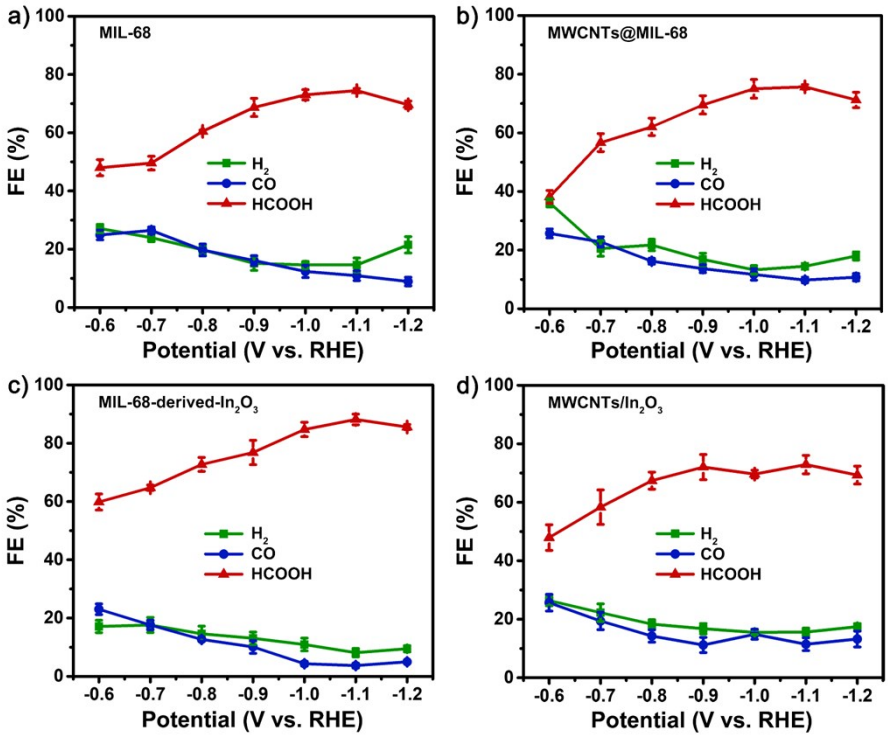

Fig. S11 FE of a) MIL-68, b) MWCNTs@MIL-68, c) MIL-68-derived-In_2O_3 and d) MWCNTs/In_2O_3.

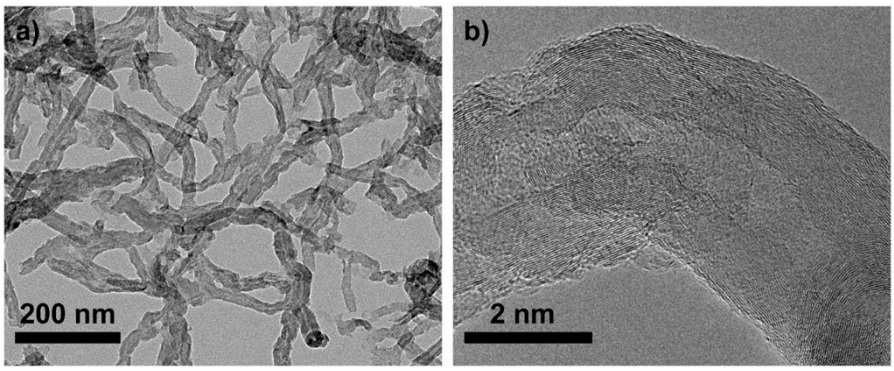

Fig. S12 a) TEM image and b) high-resolution TEM image of MWCNTs.

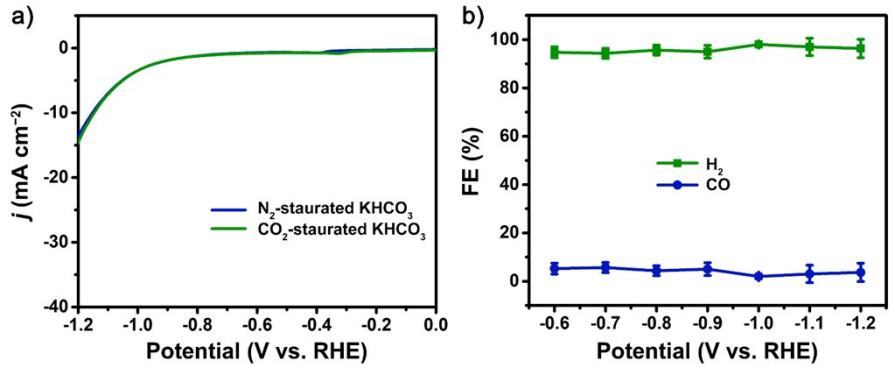

Fig. S13 a) LSV curves and b) FE of MWCNTs.

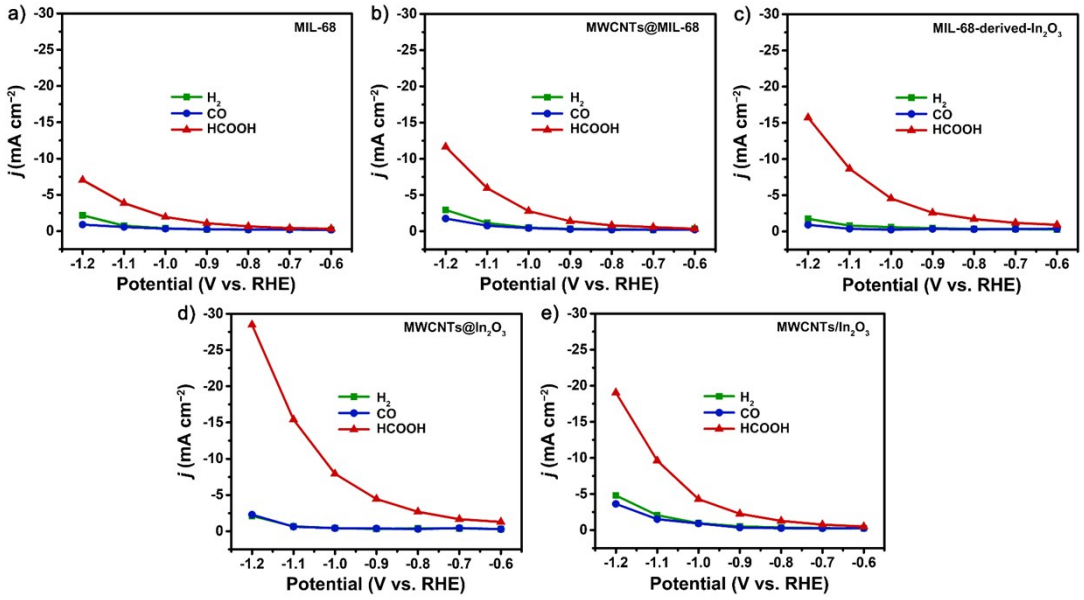

Fig. S14 Partial current density of a) MIL-68, b) MWCNTs@MIL-68, c) MIL-68-derived-In_2O_3, d) MWCNTs@In_2O_3 and e) MWCNTs/In_2O_3.

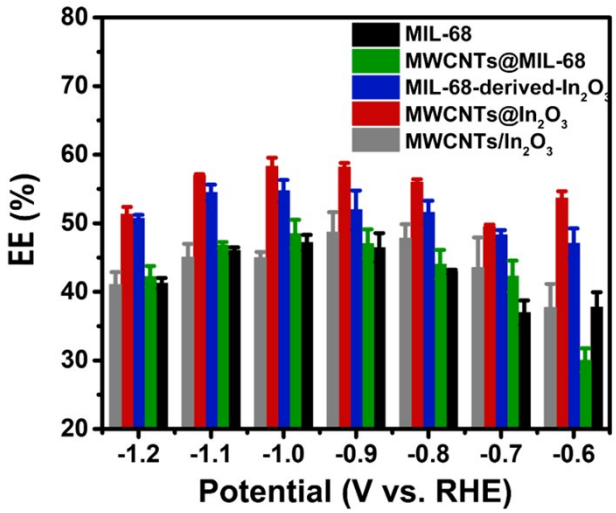

Fig. S15 Energy efficiency (EE) of MIL-68, MWCNTs@MIL-68, MIL-68-derived-In_2O_3, MWCNTs@In_2O_3 and MWCNTs/In_2O_3.

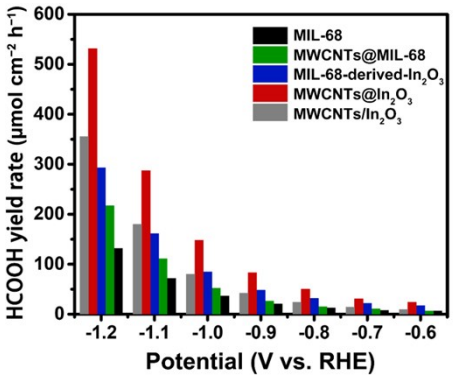

Fig. S16 HCOOH yield rate of MIL-68, MWCNTs@MIL-68, MIL-68-derived-In_2O_3, MWCNTs@In_2O_3 and MWCNTs/In_2O_3.

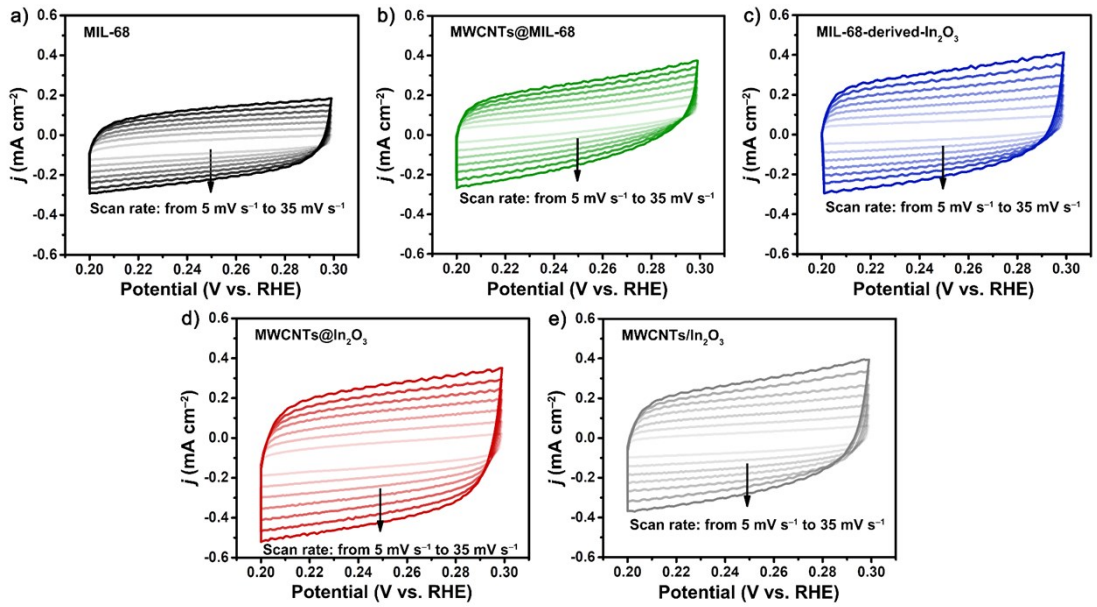

Fig. S17 Cyclic voltammograms curves of a) MIL-68, b) MWCNTs@MIL-68, c) MIL-68-derived-In_2O_3, d) MWCNTs@In_2O_3 and e) MWCNTs/In_2O_3.

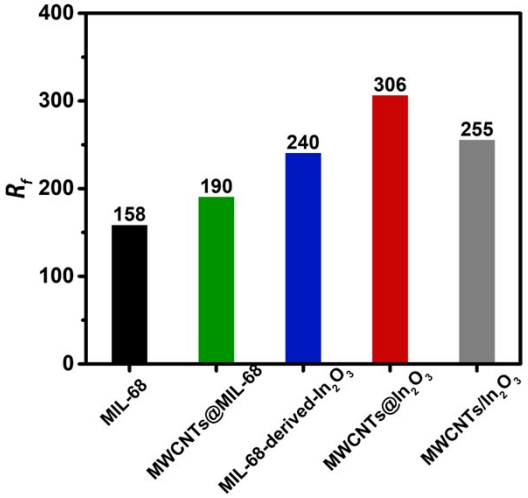

Fig. S18 R_f of MIL-68, MWCNTs@MIL-68, MIL-68-derived-In_2O_3, MWCNTs@In_2O_3 and MWCNTs/In_2O_3.

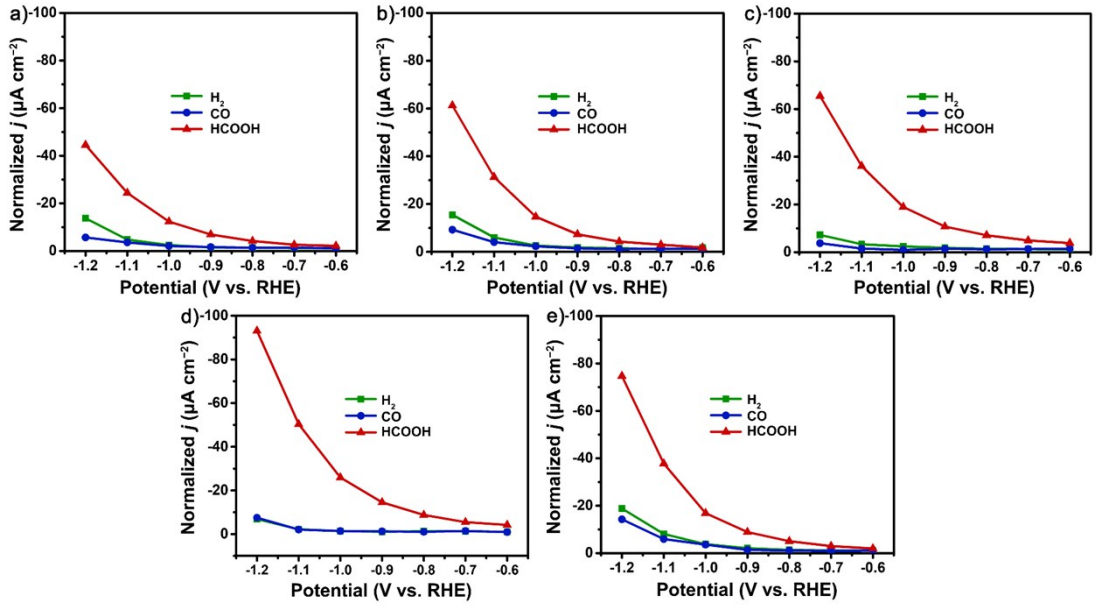

Fig. S19 ECSA-normalized partial current density of a) MIL-68, b) MWCNTs@MIL-68, c) MIL-68-derived-In_2O_3, d) MWCNTs@In_2O_3 and e) MWCNTs/In_2O_3.

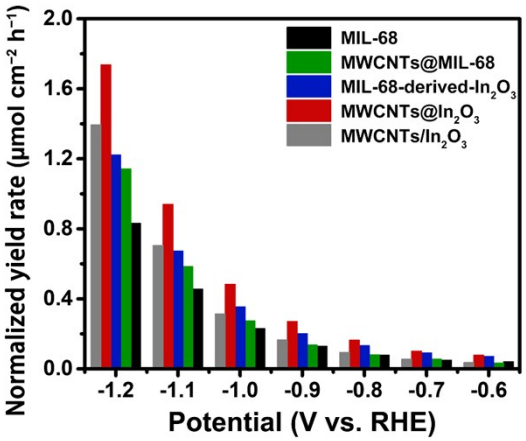

Fig. S20 ECSA-normalized HCOOH yield rate of MIL-68, MWCNTs@MIL-68, MIL-68-derived-In_2O_3, MWCNTs@In_2O_3 and MWCNTs/In_2O_3.

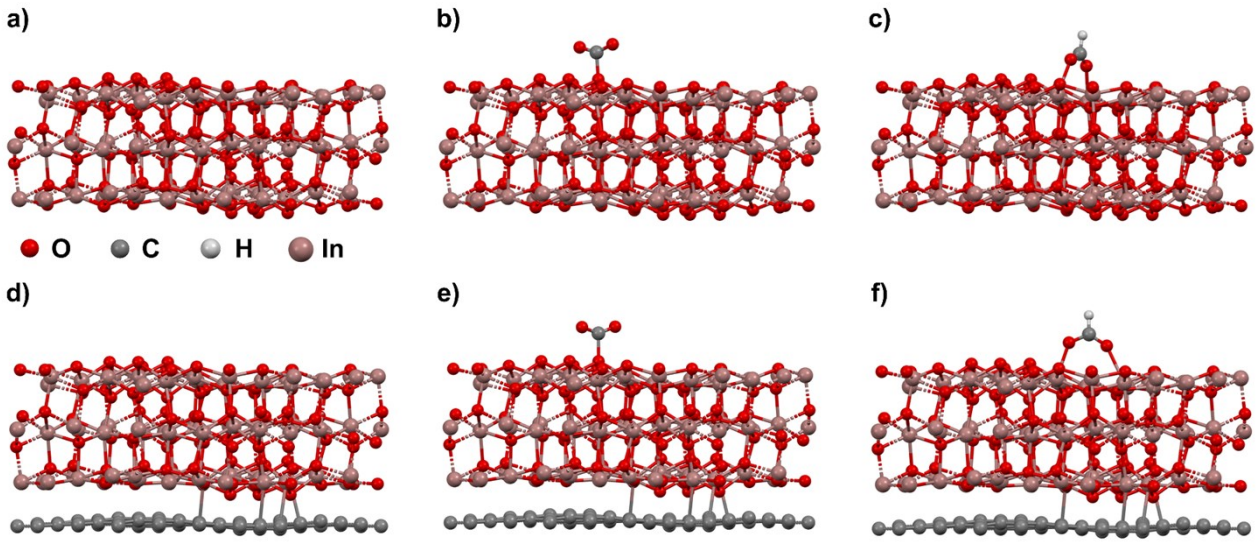

Fig. S21 a) and d) Crystal structure model of In_2O_3 and MWCNTs@In_2O_3, respectively. b) and e) Configuration of CO_2*$^-$ adsorption of In_2O_3 and MWCNTs@In_2O_3, respectively. c) and f) Configuration of HCOO*$^-$ of In_2O_3 and MWCNTs@In_2O_3, respectively.

Supplementary Table

Table S1. Comparison of the performance of eCO_2RR on different catalysts.

Catalyst	Product	*E* (V vs. RHE)	$j_{product}$ (mA cm^{-2})	*FE* (%)	*EE* (%)	Yield rate (μmol cm^{-2} h^{-1})	Ref
Bi_2O_3-NGQDs	HCOOH	−1.21	−29.3	90.8	53.6	546.6	8
SnS_2-rGO	HCOOH	−0.89	−11.7	84.5	57.4	218.3	9
$SrSnO_3$ NWs	HCOOH	−1.1	−17.3	80.5	49.8	332.7	10
Zn_2SnO_4/SnO_2	HCOOH	−1.08	−5.72	77.0	48.0	106.7	11
CuSnNWs/C-Air	HCOOH	−1.0	−17.33	90.2	58.1	323.3	12
H-InO_xNRs	HCOOH	−0.8	−7.0	90.2	63.9	130.6	13
$Ag_{76}Sn_{24}$	HCOOH	−0.8	−15.6	80.0	56.3	291.0	14
Sn-pNWs	HCOOH	−0.8	−4.8	80.1	56.4	89.6	15
Dendritic $Cu_{0.2}In_{0.8}$	HCOOH	−1.0	−0.73	62.0	36.7	13.62	16
SnO_2 QWs	HCOOH	−1.16	−13.7	88.0	53.1	255.6	17
In_2O_3-rGO	HCOOH	−1.2	−22.2	84.6	50.1	414.1	18
Bi_2O_3NSs@MCCM	HCOOH	−1.26	−15.0	93.8	54.3	279.0	19
NiSA-N-CNTs	CO	−0.7	−23.2	91.3	64.7	432.7	20
CoPc/CNT	CO	−0.63	−10.0	92.0	67.6	186.6	21
MWCNTs@In_2O_3		−1.0	−7.9	90.3	58.3	147.9	This work
		−1.1	−15.4	92.2	57.0	287.4	
		−1.2	−28.5	86.7	51.3	531.5	

Table S2. The correction of zero-point energy, enthalpy effect and entropy effect of the adsorbed and gaseous species.

	ZPE (eV)	$\int C_P dT$ (eV)	TS (eV)
HCOO*	0.62	0.10	–0.23
CO_2	0.31	0.10	0.65
HCOOH	0.90	0.11	–1.02

References

1. G. Kresse and J. Furthmüller, *Phys. Rev. B*, 1996, **54**, 11169-11186.
2. G. Kresse and J. Hafner, *Phys. Rev. B*, 1994, **49**, 14251-14269.
3. P. E. Blöchl, *Phys. Rev. B*, 1944, **50**, 17953-17979.
4. J. P. Perdew, K. Burke and M. Ernzerhof, *Physi. Rev. Lett.*, 1996, **77**, 3865-3868.
5. Y. Zhang and W. Yang, *Phys.l Rev. Lett.*, 1998, **80**, 890-890.
6. B. Hammer, L. B. Hansen and J. K. Nørskov, *Phys. Rev. B*, 1999, **59**, 7413-7421.
7. J. K. Nørskov, J. Rossmeisl, A. Logadottir, L. Lindqvist, J. R. Kitchin, T. Bligaard and H. Jónsson, *J. Phys. Chem. B*, 2004, **108**, 17886-17892.
8. Z. Chen, K. Mou, X. Wang and L. Liu, *Angew. Chem. Int. Ed.* , 2018, **57**, 12790-12794.
9. F Li, L. Chen, M. Xue, T. Williams, Y. Zhang, D. R. MacFarlane and J. Zhang, *Nano Energy*, 2017, **31**, 270-277.
10. Y. Pi, J. Guo, Q. Shao and X. Huang, *Nano Energy*, 2019, **62**, 861-868.
11. K. Wang, D. Liu, P. Deng, L. Liu, S. Lu, Z. Sun, Y. Ma, Y. Wang, M. Li, B. Y. Xia, C. Xiao and S. Ding, *Nano Energy*, 2019, **64**, 103954.
12. J. Wang, Y. Ji, Q. Shao, R. Yin, J. Guo, Y. Li and X. Huang, *Nano Energy*, 2019, **59**, 138-145.
13. J. Zhang, R. Yin, Q. Shao, T. Zhu and X. Huang, *Angew. Chem. Int. Ed.* , 2019, **58**, 5609-5613.
14. W. Luc, C. Collins, S. Wang, H. Xin, K. He, Y. Kang and F. Jiao, *J. Am. Chem. Soc.*, 2017, **139**, 1885-1893.
15. B. Kumar, V. Atla, J. P. Brian, S. Kumari, T. Q. Nguyen, M. Sunkara and J. M. Spurgeon, *Angew. Chem. Int. Ed.* , 2017, **56**, 3645-3649.
16. Z. B. Hoffman, T. S. Gray, K. B. Moraveck, T. B. Gunnoe and G. Zangari, *ACS Catal.*, 2017, **7**, 5381-5390.
17. S. Liu, J. Xiao, X. F. Lu, J. Wang, X. Wang and X. W. D. Lou, *Angew. Chem. Int. Ed.* , 2019, **58**, 8499-8503.
18. Z. Zhang, F. Ahmad, W. Zhao, W. Yan, W. Zhang, H. Huang, C. Ma and J. Zeng, *Nano Lett.*, 2019, **19**, 4029-4034.
19. S. Liu, X. F. Lu, J. Xiao, X. Wang and X. W. D. Lou, *Angew. Chem. Int. Ed.*, 2019, **58**, 13828-13833.
20. Y. Cheng, S. Zhao, B. Johannessen, J. P. Veder, M. Saunders, M. R. Rowles, M. Cheng, C. Liu, M. F. Chisholm, R. De Marco, H. M. Cheng, S. Z. Yang and S. P. Jiang, *Adv. Mater.*, 2018, **30**, e1706287.
21. X. Zhang, Z. Wu, X. Zhang, L. Li, Y. Li, H. Xu, X. Li, X. Yu, Z. Zhang, Y. Liang and H. Wang, *Nat. Commun.*, 2017, **8**, 14675.